Geophysical Research Letters

RESEARCH LETTER
10.1029/2018GL080963

Special Section:
Bridging Weather and Climate: Subseasonal-to-Seasonal (S2S) Prediction

Late-July Barrier for Subseasonal Forecast of Summer Daily Maximum Temperature Over Yangtze River Basin

Jing Yang[1,2], Tao Zhu[1], Miaoni Gao[3], Hai Lin[4], Bin Wang[5], and Qing Bao[6]

[1]State Key Laboratory of Earth Surface Processes and Resource Ecology/Academy of Disaster Reduction and Emergency Management Ministry of Civil Affairs and Ministry of Education, Faculty of Geographical Science, Beijing Normal University, Beijing, China, [2]Atmospheric Sciences Research Center, State University of New York at Albany, Albany, NY, USA, [3]School of Systems Science, Beijing Normal University, Beijing, China, [4]Meteorological Research Division, Environment and Climate Change Canada, Dorval, Quebec, Canada, [5]Department of Atmospheric Sciences, and International Pacific Research Center, University of Hawai'i at Mānoa, Honolulu, HI, USA, [6]State Key Laboratory of Numerical Modeling for Atmospheric Sciences and Geophysical Fluid Dynamics (LASG), IAP/CAS, Beijing, China

Abstract Dynamical subseasonal forecast skill of summer daily maximum temperature (T_{max}) over East China was evaluated based on a 20-year (1995–2014) subseasonal reforecast data set from the European Centre for Medium-range Weather Forecasts. A significant late-July barrier of subseasonal forecast skill was identified for the T_{max} over the Yangtze River Basin, which concurs with a reduction in the prediction skill for the local 500-hPa geopotential height. This barrier period corresponds to an abrupt transitional phase of the climatological intraseasonal oscillation when the western North Pacific subtropical high abruptly migrates northward from Yangtze River Basin to northern China. The transitional phase of the climatological intraseasonal oscillation features the largest day-to-day variance in the position of western North Pacific subtropical high, which may cause the drop of the subseasonal forecast skill for both the geopotential height and T_{max}. The results indicate that the atmospheric subseasonal predictability may be strongly affected by the phases of the local climatological intraseasonal variation.

Plain Language Summary This study identified a significant late-July barrier of subseasonal forecast skill over the Yangtze River Basin and suggested that the atmospheric subseasonal predictability may be strongly affected by the phases of the local climatological intraseasonal variation.

Key Points:
- A significant late-July barrier of subseasonal forecast skill was identified for the EHT over the Yangtze River Basin
- This barrier period corresponds to an abrupt transitional phase of the CISO when the WNPSH abruptly migrates northward
- The atmospheric subseasonal predictability may be strongly affected by the phases of the local climatological ISV

Supporting Information:
- Supporting Information S1

Correspondence to:
J. Yang,
yangjing@bnu.edu.cn

Citation:
Yang, J., Zhu, T., Gao, M., Lin, H., Wang, B., & Bao, Q. (2018). Late-July barrier for subseasonal forecast of summer daily maximum temperature over Yangtze River Basin. *Geophysical Research Letters*, *45*, 12,610–12,615. https://doi.org/10.1029/2018GL080963

Received 5 SEP 2018
Accepted 3 NOV 2018
Accepted article online 9 NOV 2018
Published online 23 NOV 2018

1. Introduction

The occurrence of heat waves in China has increased significantly as a result of global warming (e.g., T. Ding & Ke, 2015; You et al., 2016), with potentially disastrous impacts on health and economy. Reliable weather and climate forecasts for extreme high temperature (EHT) are important for both early warning systems and risk mitigation (National Academies of Sciences, Engineering, and Medicine, 2016). There is currently a forecast gap for time scales ranging from 1 week to 1 month. This is considered to be the most challenging time scale because many of the initial signals in the atmosphere are almost lost, but the lower boundary conditions have not yet taken full effect (Liang & Lin, 2017).

Since one source for the subseasonal prediction of EHT is the atmospheric intraseasonal oscillation (Gao et al., 2017; Yang et al., 2010), some previous studies have attempted to forecast EHT by detecting statistical intraseasonal precursory signals (T. Ding & Qian, 2012; Teng et al., 2013) and producing statistical subseasonal forecast models of heat waves (Zhu & Li, 2017). However, even a state-of-the-art statistical subseasonal model can only capture nearly 30% of the heat waves over China with a 15-day lead time (Zhu & Li, 2017). In comparison, with improved general circulation models and forecast techniques, the current numerical dynamical models have shown an increasing capability in producing skillful forecasts for extreme events on subseasonal time scales (Mariotti et al., 2018). The World Weather Research Programme and World Climate Research Programme subseasonal to seasonal (S2S) prediction project (Vitart et al., 2017), with a special emphasis on high-impact weather events, have made available a large database and provided a new opportunity for evaluating the current subseasonal prediction skill for EHT in current dynamic models.

Therefore, it is of great interest to assess the subseasonal prediction skill of EHT over its core region of East China. Because the East China summer features a remarkable climatological intraseasonal march of the circulation (Y. H. Ding, 2005; Wang & Xu, 1997), whether the subseasonal prediction skill of EHT is influenced by the

phases of the climatological subseasonal march is worthwhile to investigate. Primarily based on the S2S reforecast data sets of the European Centre for Medium-Range Weather Forecasts (ECMWF) from the S2S database, a varying subseasonal prediction skill is reported and its associated cause is also discussed.

2. Data Sets and Method

Because the daily maximum temperature at 2 m (T_{max}) is the most important indicator for the EHT events (e.g., Fischer & Schär, 2010), this study mainly focused on the prediction skill of T_{max}. The T_{max} for the reforecast of the ECMWF subseasonal forecast system was retrieved from the S2S prediction project database (Vitart et al., 2017). The ECMWF subseasonal prediction system initializes the reforecasts every Monday and Thursday, with 10 ensemble members initialized on the same calendar date for the 20-year reforecast period of 1995–2014 (i.e., an *on-the-fly* method). Each reforecast lasts 47 days. To verify the reliability of the major finding, we also examined the prediction results from other two models of China (see supporting information Figure S1).

The observed T_{max} is from the CN05.1 data set, which is provided by the Chinese National Climate Center, and has a spatial resolution of 0.25° (Wu & Gao, 2013; Xu et al., 2009). The T_{max} data from 2000 gauge stations over China from the China Meteorological Administration are also used to confirm the reliability of the result (not shown). The observed atmospheric circulation is represented by the ERA-Interim reanalysis data (Dee et al., 2011). The selected observational period is similar to the reforecast.

For each year from 1995 to 2014, the variable anomalies in the reforecast data were calibrated by removing the ensemble mean model climate. The model climate was calculated in a cross-validated way by excluding the year of the anomaly. The reforecast anomaly is essentially a function of both the lead time and the initialization date. The same procedure was applied to the observation to obtain the observed anomalies.

To investigate the temporal variation of subseasonal prediction skill, we utilized a time window of 11 target days and calculate the temporal correlation coefficients (TCCs) between the observation and the corresponding forecasts for these target days at different lead times over the 20 peak seasons (a total of $11 \times 20 = 220$ forecasts) to represent the correlation skill of the targeted middle date (day 6). We slide the 11-day segment one day forward with the middle date (day 6) moving from 1 July to 31 August to calculate the skill for each day. This roughly represents a day-to-day variation of running mean subseasonal prediction correlation skill (called skill hereafter) during a specific season. We also examined the result using other windows (e.g., 9-day) and the following major findings are not sensitive to different windows (see supporting information Figure S2). We applied the Chiclet diagram to illustrate the change in prediction skill as a function of lead time and starting date (Carbin et al., 2016). For the convenience of calculating and illustrating the results, we have preprocessed the ECMWF's twice-weekly reforecast data so that every daily target date has its forecasts of different lead times (see supporting information Table S1 for detailed description of the procedure) and also verified that the major finding was not influenced by this special treatment (see supporting information Figure S3).

3. Subseasonal Prediction of T_{max} Over East China

3.1. The Subseasonal Prediction of the Climatology of T_{max}

Previous studies have shown that July–August (JA) is the peak season of hot days over East China (Gao et al., 2018, 2017). In the observation as shown in Figure 1a, the Yangtze River Basin (YRB) is the dominant center of T_{max} and the southern China (SC) is the second maximum center over East China during JA. In this peak season, high T_{max} mainly occurs before the mid-August as shown in Figure 1b. To evaluate the subseasonal prediction skill of T_{max} in its peak season, we examined the 20-year averaged reforecast ensemble mean T_{max} with a lead time of 2 and 3 weeks, respectively (Figures 1c–1f). The ECMWF model can realistically capture the climatological features in the core regions of T_{max} over the YRB in the peak season 2 and 3 weeks in advance. However, the prediction results have two evident biases: One is the failure of reproducing the SC maximum center and the other is a false maximum center over the North China Plain. It seems that the predicted T_{max} region shifts northward slightly, which is linked to its predicted bias in climatological position of western North Pacific subtropical high (WNPSH) (see supporting information Figure S4).

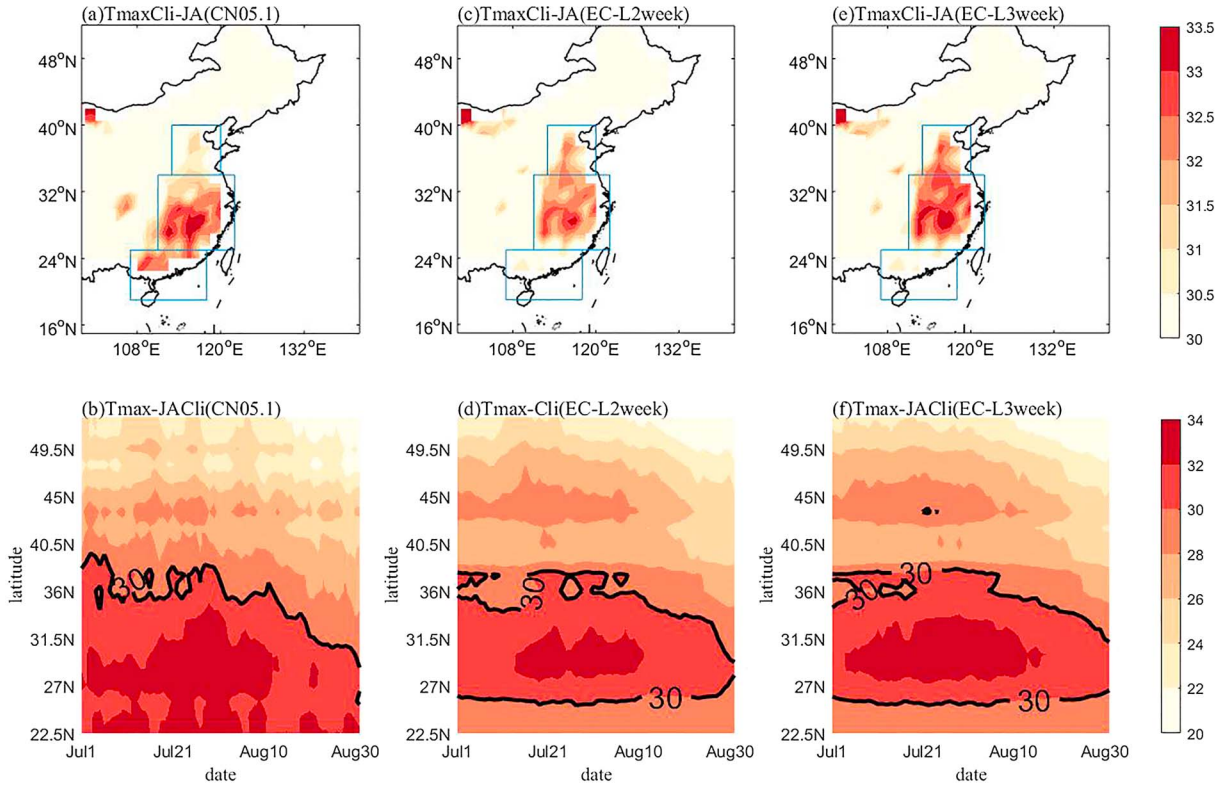

Figure 1. (a, c, and e) Spatial distribution of T_{max} (units: °C) over eastern China in July–August during 1995–2014. Blue boxes denote the North China Plain, the Yangtze River Basin, and Southern China, respectively. (b, d, and f) Evolution of zonal mean T_{max} averaged over 111–122°E from July to August. Black solid lines are 30 °C isolines. (a)(b), and (c)(d) and (e)(f) show the results in CN05.1 (observation) and the 2-week lead and 3-week lead predictions from European Centre for Medium-range Weather Forecasts, respectively.

Therefore, the YRB core region has the best prediction compared with the other two regions in this subseasonal forecast system. Over the core region, the warmest period is from early July to mid-August in the observation. In the reforecast, the warmest period can be well predicted even with a lead of 3 weeks. Therefore, the ECMWF model is able to capture the major climatological spatial-temporal features of the T_{max} over the core region of East China.

3.2. The Late-July Barrier of Subseasonal Prediction Skill of T_{max} Over the YRB

Figure 2a presents a Chiclet diagram of the ensemble mean TCC, which demonstrates how the prediction skill changes with the target date and lead time. Of great interest is that the prediction skill is not stable during the peak season. The most remarkable feature is a sharp decline of prediction skill in late July (with a minimum around 21 July). Here we refer to the salient reduction of prediction skill in late July as the late-July prediction barrier. This barrier can also be seen in the subseasonal reforecasts of the other two models (see supporting information model descriptions).

Again, we calculated the temporal change of predictable days in this season. If TCC of the *N*-day lead reforecast cannot pass the 95% confidence level for the first time, we define $N-1$ day as the predictable days of the middle date (day 6). Figure 2b shows that the predictable days abruptly drop down to 8 days around 21 July, while the prediction skill reaches 10–15 days before and after the barrier.

In addition, we examined the prediction skill of EHT through some common methods (e.g., Zhu & Li, 2017). We applied the hit rate (HR) of the hot days to measure the prediction skill. We used a relative definition of heat wave to select hot days in both observation and prediction. The hot day refers to a day with T_{max} exceeding the calendar day 90th percentile centered on a 15-day window for the whole period (1995–2014) (Fischer & Schär, 2010). The HR was calculated by the ratio of hot days from prediction against observation of 11 days centered on each calendar day from 1 July 1 to 13 August 13 during the period 1995 to 2014 in the reforecast. If the HR of the *N*-day lead reforecast is fewer than 0.5 for the first time, we defined $N-1$ day as the effective

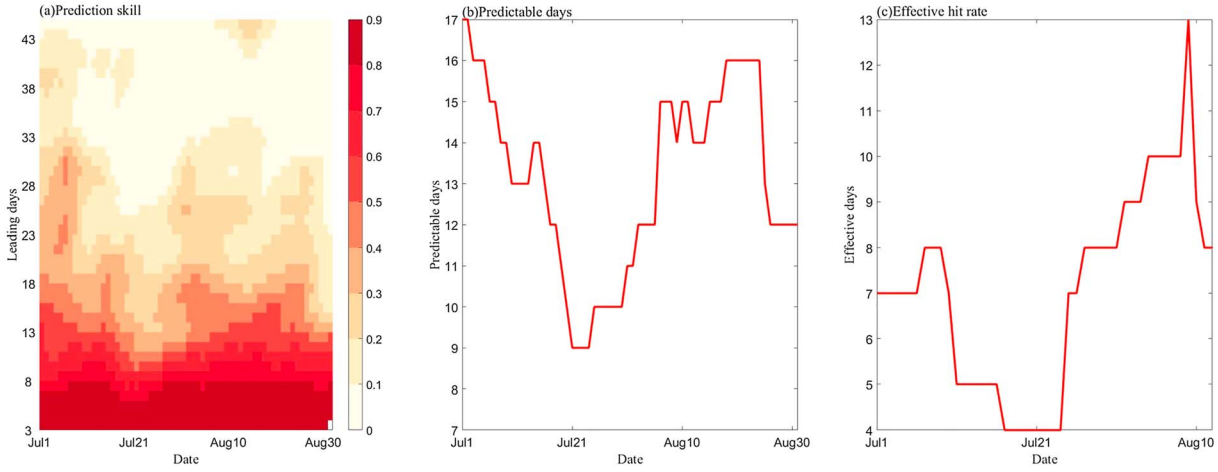

Figure 2. (a) Prediction skills and (b) predictable days for the T_{max} averaged over Yangtze River Basin of 11 days centered on each calendar day from 1 July to 31 August during the period 1995 to 2014 for European Centre for Medium-range Weather Forecasts, as a function of the date (horizontal axis) and (a) lead time/(b) predictable days (vertical axis). (c) Effective hit rate for the hot days over Yangtze River Basin of 11 days centered on each calendar day from 1 July to 13 August during the period 1995 to 2014 for European Centre for Medium-range Weather Forecasts.

HR days of the middle date (day 6). As a result, a sharp decline of HR can be also exhibited in late July shown as in Figure 2c.

4. Discussion: Cause for the Subseasonal Forecast Barrier

Previous studies have reported that T_{max} in the YRB is closely related to the downward motion near the ridge of the WNPSH (e.g., Gu et al., 2016; Peng, 2014). We therefore examined the day-to-day relationship between the YRB area-averaged T_{max} anomaly and the daily 500-hPa geopotential height (GHT500) at each grid point during the 20 reforecast years (Figure 3a). Figure 3a does show that the maximum positive correlation is located over the YRB during JA. To understand the late-July prediction barrier over the YRB at the subseasonal time scale, we made an analysis similar to that in Figure 2 for the correlation skill of GHT500 (Figure 3b). The results show that the prediction skill of GHT500 in late July is also the lowest, suggesting that the prediction skill of T_{max} and that of GHT500 are closely correlated in boreal summer.

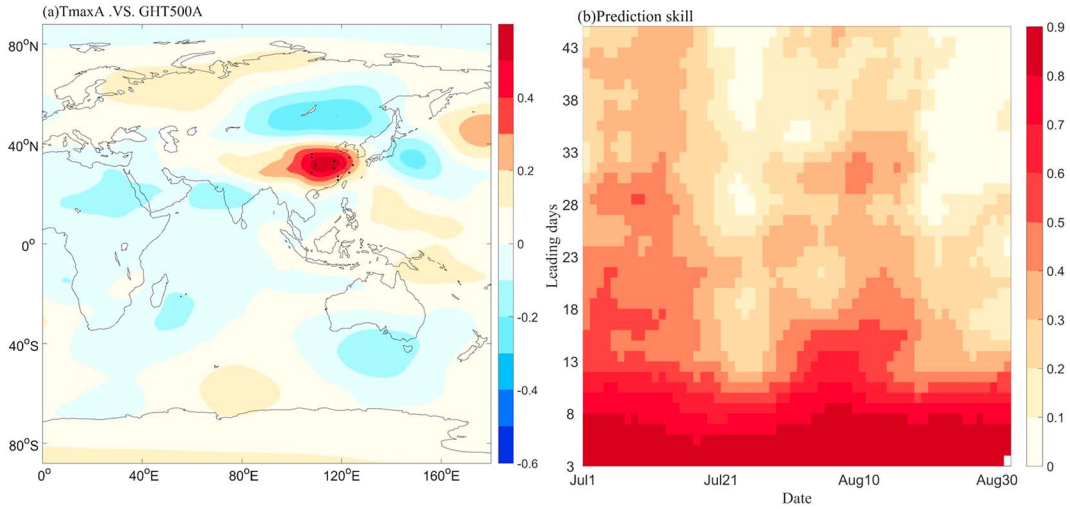

Figure 3. (a) Correlation coefficients between observed T_{max} averaged over Yangtze River Basin and 500-hPa geopotential height anomalies at each grid point in July–August during the period 1995–2014. Black dotes denote the values significant at 99% confidence level. (b) The same as Figure 2a but for 500-hPa geopotential height.

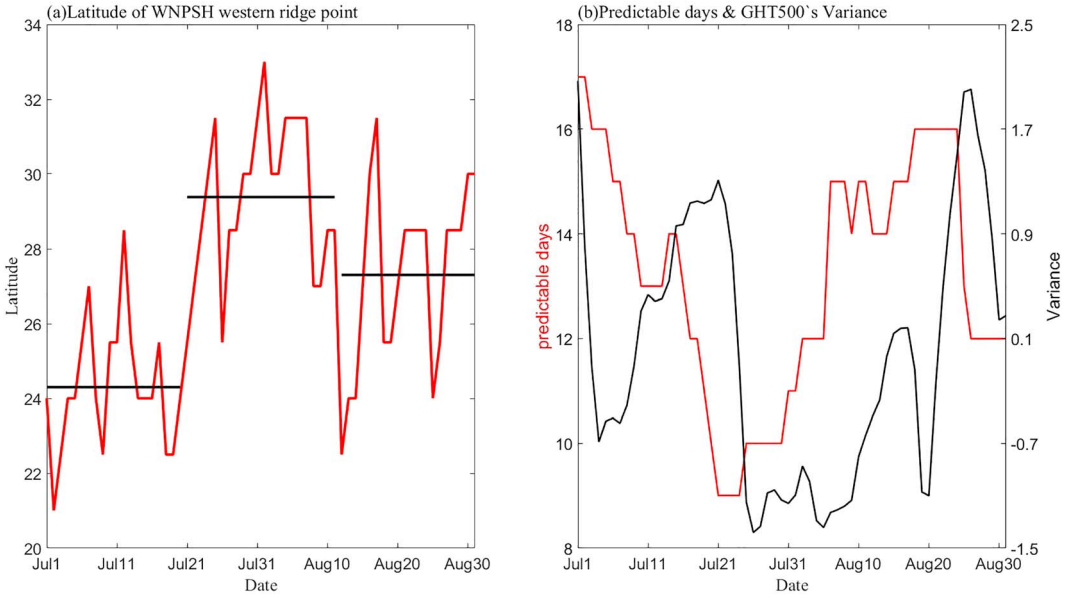

Figure 4. (a) Evolution of latitudes of WNPSH western ridge point from 1 July to 31 August in 1995–2014. Black solid lines represent the averages of the period 1–20 July, 21 July to 10 August, and 11–31 August, respectively. (b) The 11-day running variance of 500-hPa geopotential height anomalies averaged over the domain (25–37°N, 104–125°E) in Figure 3 centered on each calendar day from 1 July to 31 August during the period 1995 to 2014 (black lines) and the predictable days (red lines), which are same as Figure 2b. The *x* axis represents the middle date (6th) of each 11-day running mean time series. WNPSH = western North Pacific subtropical high.

The GHT500 variation subseasonal progression of the WNPSH is closely related to the climatological intraseasonal oscillation (CISO) of the East Asian-western North Pacific monsoon (Wang & Xu, 1997). Figure 4a shows the northward migration of WNPSH that is represented by the latitude of its western ridge point, defined as the latitude of the westernmost position of 5,880-gpm isoline in the area (10–60°N, 90–180°E) in boreal summer. Obviously, the abrupt northward migration of the climatological WNPSH just occurs in the beginning of late July around 21 July, which is consistent with previous studies (e.g., Wang & Xu, 1997). The abrupt jump is actually a manifestation of the swift transitional phase of the CISO. Figure 4b shows that the WNPSH experiences the largest day-to-day variance around 21 July, right before this abrupt transitional phase. The large day-to-day variability around 21 July can potentially increase the prediction uncertainty and reduce the predictability of T_{max}. It is also possible that the transitional phase of the CISO provides an environment, which leads to atmospheric variability of chaotic nature and less predictable. Therefore, the late-July barrier can be remarkably detected in the subseasonal prediction of T_{max} over the YRB.

5. Conclusions

Based on the ECMWF subseasonal reforecast results, we evaluated the subseasonal prediction skill for T_{max} in its peak season, July and August over East China. The YRB region is the core region of T_{max} in East China. The 2- and 3-week lead forecasts of ECMWF capture the climatological feature of T_{max} the best over YRB (Figure 1). The most remarkable finding is the existence of a significant late-July barrier for subseasonal prediction skill of T_{max} over the YRB. It is found that there is a high day-to-day correlation between the T_{max} and the GHT500 over the YRB, and a sharp reduction in the GHT500 prediction skill also appears in the barrier period.

Further analysis reveals that the late July is a climatologically rapid transitional phase of the CISO, during which the WNPSH experiences an abrupt northward migration. The transitional phase of CISO corresponds to the period when the position of the WNPSH has the largest day-to-day variance. It is conceivable that the drop of prediction skill results from the abrupt change in the WNPSH at the swift transition of CISO and the associated large amplitude of internal variability. The finding indicates that the atmospheric subseasonal predictability can change significantly due to the phase locking of intraseasonal oscillation to the annual cycle.

Acknowledgments

This study was supported by funds from and National Natural Science Foundation of China (Grants 41775071, 91637312, and 41621061) and the National Key Research and Development Program-Global Change and Mitigation Project: Global Change Risk of Population and Economic System: Mechanism and Assessment (Grant 2016YFA0602401). The T_{max} of gridded stations data are from the China Meteorological Administration (IP: 59.64.36.30: ~/mnt/storage-3/CN05.1_1961-2015). The T_{max} data from 2000 gauge stations over China are also from the China Meteorological Administration (IP: 59.64.36.30: ~/home/zhutao/data/TEM). The ERA-Interim data can be freely downloaded from http://apps.ecmwf.int/datasets/data/interim-full-daily/levtype=sfc/. The ECMWF/CMA reforecast data set can be accessed on http://apps.ecmwf.int/datasets/data/s2s-reforecasts-daily-averaged-ecmf/levtype=sfc/type=cf/. The FGOALS-f2 reforecast data set can be accessed (IP: 59.64.36.30: ~/mnt/storage-60 T/fgoals-S2S-zt/s2s_t_zg500/s2s_t2m).

References

Carbin, G. W., Tippett, M. K., Lillo, S. P., & Brooks, H. E. (2016). Visualizing long-range severe thunderstorm environment guidance from CFSv2. *Bulletin of the American Meteorological Society*, *97*(6), 1021–1031. https://doi.org/10.1175/BAMS-D-14-00136.1

Dee, D. P., Uppala, S. M., Simmons, A. J., Berrisford, P., Poli, P., Kobayashi, S., Andrae, U., et al. (2011). The ERA-Interim reanalysis: configuration and performance of the data assimilation system. *Quarterly Journal of the Royal Meteorological Society*, *137*(656), 553–597. https://doi.org/10.1002/qj.828

Ding, T., & Ke, Z. (2015). Characteristics and changes of regional wet and dry heat wave events in china during 1960–2013. *Theoretical and Applied Climatology*, *122*(3–4), 651–665. https://doi.org/10.1007/s00704-014-1322-9

Ding, T., & Qian, W. (2012). Statistical characteristics of heat wave precursors in China and model prediction. *Chinese Journal of Geophysics*, *55*(5), 1472–1486. https://doi.org/10.6038/j.issn.0001-5733.2012.05.005

Ding, Y. H. (2005). *Advanced synoptic meteorology*, (p. 585). Beijing: China Meteorological Press.

Fischer, E. M., & Schär, C. (2010). Consistent geographical patterns of changes in high-impact European heatwaves. *Nature Geoscience*, *3*(6), 398–403. https://doi.org/10.1038/ngeo866

Gao, M., Wang, B., Yang, J., & Dong, W. (2018). Are peak summer sultry heat wave days over Yangtze-Huaihe river basin predictable? *Journal of Climate*, *31*(6), 2185–2196. https://doi.org/10.1175/JCLI-D-17-0342.1

Gao, M., Yang, J., Wang, B., Zhou, S., Gong, D., & Kim, S. J. (2017). How are heat waves over Yangtze River valley associated with atmospheric quasi-biweekly oscillation? *Climate Dynamics*, 1–17. https://doi.org/10.1007/s00382-017-3526-z

Gu, B., Zheng, Z., Feng, G., & Wang, X. (2016). Interdecadal transition in the relationship between the western pacific subtropical high and sea surface temperature. *International Journal of Climatology*, *37*(5), 2667–2678. https://doi.org/10.1002/joc.4872

Liang, P., & Lin, H. (2017). Sub-seasonal prediction over East Asia during boreal summer using the ECCC monthly forecasting system. *Climate Dynamics*, *50*(3-4), 1007–1022. https://doi.org/10.1007/s00382-017-3658-1

Mariotti, A., Ruti, P. M., & Rixen, M. (2018). Progress in subseasonal to seasonal prediction through a joint weather and climate community effort. *Climate and Atmospheric Science*, *1*(1). https://doi.org/10.1038/s41612-018-0014-z

National Academies of Sciences, Engineering, and Medicine (2016). *Attribution of extreme weather events in the context of climate change*. Washington, DC: The National Academies Press. https://doi.org/10.17226/21852

Peng, J. B. (2014). An investigation of the formation of the heat wave in southern China in summer 2013 and the relevant abnormal subtropical high activities. *Atmospheric and Oceanic Science Letters*, *7*(4), 286–290. https://doi.org/10.3878/j.issn.1674-2834.13.0097

Teng, H., Branstator, G., Wang, H., Meehl, G. A., & Washington, W. M. (2013). Probability of US heat waves affected by a subseasonal planetary wave pattern. *Nature Geoscience*, *6*(12), 1056–1061. https://doi.org/10.1038/NGEO1988

Vitart, F., Ardilouze, C., Bonet, A., Brookshaw, A., Chen, M., Codorean, C., Déqué, M., et al. (2017). The subseasonal to seasonal (S2S) prediction project database. *Bulletin of the American Meteorological Society*, *98*(1), 163–173.https://doi.org/10.1175/BAMS-D-16-0017.1

Wang, B., & Xu, X. (1997). Northern Hemisphere summer monsoon singularities and climatological intraseasonal oscillation. *Journal of Climate*, *10*(10), 1071–1085. https://doi.org/10.1175/1520-0442(1997)010<1071:NHSMSA>2.0.CO;2

Wu, J., & Gao, X. (2013). A gridded daily observation dataset over China region and comparison with the other datasets. *Chinese Journal of Geophysics*, *56*(4), 1102–1111. https://doi.org/10.6038/cjg20130406

Xu, Y., Gao, X., Yan, S., Xu, C., Ying, S., & Giorgi, F. (2009). A daily temperature dataset over China and its application in validating a RCM simulation. *Advances in Atmospheric Sciences*, *26*(4), 763–772. https://doi.org/10.1007/s00376-009-9029-z

Yang, J., Wang, B., & Bao, Q. (2010). Biweekly and 21-30-day variations of the subtropical summer monsoon rainfall over the lower reach of the Yangtze River Basin. *Journal of Climate*, *23*(5), 1146–1159. https://doi.org/10.1175/2009JCLI3005.1

You, Q., Jiang, Z., Kong, L., Wu, Z., Bao, Y., Kang, S., & Pepin, N. (2016). A comparison of heat wave climatologies and trends in China based on multiple definitions. *Climate Dynamics*, *48*(11–12), 3975–3989.https://doi.org/10.1007/s00382-016-3315-0

Zhu, Z., & Li, T. (2017). Extended-range forecasting of Chinese summer surface air temperature and heat waves. *Climate Dynamics*, *50*(5-6), 2007–2021. https://doi.org/10.1007/s00382-017-3733-7